Article

Enhanced diclofenac photomineralization under solar light using $Ce_{1-x}Zn_xO_{2-x}$ solid solution catalysts: synergistic effect of photoexcited electrons and oxygen vacancies

Meryem Abbadi[1,2], Aimé Victoire Abega[1], Christian Brice Dantio Nguela[1], Abdelaziz Laghzizil[2] and Didier Robert[1]

[1]Institut de Chimie et Procédés pour l'Energie, l'Environnement et la Santé (ICPEES), CNRS University of Strasbourg, Saint-Avold Antenna, Université de Lorraine rue Victor Demange, Rue Victor Demange, 57500, Saint-Avold, France

[2]Laboratory of Applied Chemistry of Materials, Faculty of Science, Mohammed V University in Rabat, Avenue Ibn Batouta BP.1014, Rabat Morocco

Abstract: The present work describes the synthesis, characterization and photomineralization activity of synthesized $Ce_{1-x}Zn_xO_{2-x}$ solid solution catalysts allowing the degradation of Diclofenac as a model of anti-inflammatory medicines in water. Oxygen deficient photocatalysts $Ce_{1-x}Zn_xO_{2-x}$ (CeZnx), produced with mixing ZnO and CeO_2 have been characterized for their crystallographic parameters, specific surface area and morphology. Photomineralization activity determinations using TOC analysis have shown efficient diclofenac photooxidation under sunlight. Moreover, results indicate that coexistence of Zn^{2+}, Ce^{4+} and oxygen vacancies rate in CeZnx solid solution are key factors for strong drug mineralization. Finally, CeZn0.1 which is one of the photocatalysts synthesized in the present work represents a cheap and efficient reagent for organic matter photomineralization in wastewater.

Keywords. CeO_2; $Ce_{1-x}Zn_xO_{2-x}$ solid solution; diclofenac; photomineraliztion**;** oxygen vacancies effect

1. Introduction

Detection of pharmaceutical residues in aquatic environments is a major concern because of their potential impacts on ecosystems and human health [1]. Pharmaceuticals end up in wastewater through several ways, as follows: fecal excretion of medicines and their metabolites by patients; care facilities untreated effluents which are released into rivers and carried over to STEPs; industrials effluents from pharmaceuticals production sites. Although in developed countries, such effluents undergo an on-site wastewater treatment before being released into rivers, in emerging countries which produce numerous generics, no strict regulations do currently exist for pharmaceuticals removal before their environmental release. Hence, wastewaters contain various medicines, most of them being antibiotics, anti-inflammatories and analgesics. Moreover, several drug residues end-up undegraded in final STEPs effluents and are released to surface waters. Sodium diclofenac is a major pharmaceutical detected in many wastewater treatment plant effluents [2]. This medicine is a non-steroidal anti-inflammatory drug commonly used for rheumatoid arthritis and osteoarthritis [3]. It is considered as a persistent toxic substance causing adverse effects on terrestrial and aquatic flora [4]. As a result, efficient and sustainable technologies such as coagulation, flocculation, electrochemical treatment, filtration, and adsorption are urgently needed to oxidize this pollutant in wastewater. However, many of these processes have high treatment costs and are inefficient for mineralizing and completely degrading the molecule.

Many advanced oxidation processes (AOP) have been used to remove Diclofenac from wastewater [3-5]. Among them, heterogeneous photocatalysis is efficient for Diclofenac mineralization [5, 6]. Moreover, it is a sustainable, effective and non-selective water

Preprints (www.preprints.org) | NOT PEER-REVIEWED | Posted: 16 June 2023 doi:10.20944/preprints202306.1244.v1

purification and disinfection method, allowing the mineralization of most organic compounds [7]. The process is based on light absorption by semiconductors such as TiO_2, ZnO, Fe_2O_3 and CdS [7-11]. TiO_2 is the main semiconductor used in heterogeneous photocatalysis because of its high activity, stability and chemical inactivity. ZnO is an alternative to TiO_2 as it has similar properties, but it displays reduced production costs, higher electronic conductivity resulting in faster charge transfer of photogenerated species to the surface, with lower recombination rates than TiO_2 [12, 13]. However, ZnO photocatalytic properties depend on particles size, morphology [14, 15], and photocorrosion sensitivity, which limit its activity towards recalcitrant pollutants [16]. ZnO stability and reactivity can be improved with performing heterojunctions with other semiconductors [17-20]. Cerium oxide (CeO_2) is a good electron acceptor and excellent oxygen storage medium [21], showing a similar energy level (E_g) as ZnO [23]. Besides, these mineral displays high thermal stability, abundance, non-toxicity, and low cost. It has been widely applied in water-gas conversion reactions, three-way automotive catalysts, fuel cells and oxygen sensors [22]. Recent studies have reported its potential photocatalytic activity since CeO_2 shows a UV-vis response thanks to abundant oxygen vacancies, and a high redox capacity, allowing efficient oxidation of wastewater organic matter, and hydrogen production using water [23].

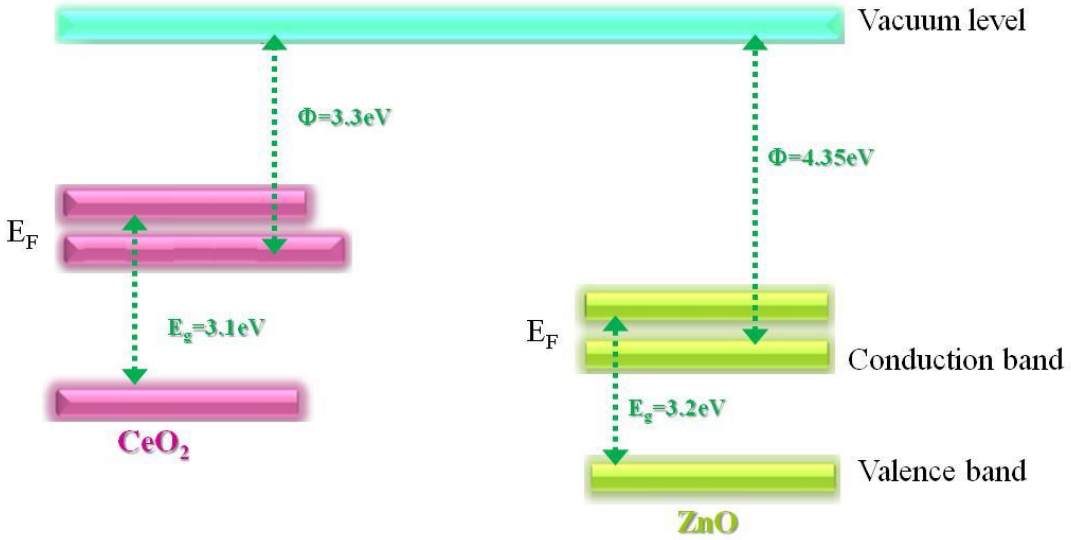

Figure 1. Energy band diagram of CeO_2 and ZnO n-type semiconducting materials.

Interfacial CeO_2-ZnO heterojunctions should be possible, due to their appropriate band structures allowing high photocatalytic efficiency with high redox capacity and efficient photoinduced charge carrier separation. Although some ZnO/CeO_2 composites have been developed for photocatalytic applications [24, 25], identification of their photocatalytic mechanism for pharmaceuticals removal in water by mineralization remains a major challenge. Intermediate products formation after photocatalysis, metal ions release, and weak bonds between the two oxides in composites appear as limiting factors for photocatalytic applications.

UV photocatalytic activity of CeO_2/ZnO composites has shown an efficiency of 67.4% for methylene blue degradation [26]. In addition, significant photocatalytic activity increase has been demonstrated by the intra-band exciton transfer, in removal of phenol and its derivatives [27]. Reports on antibiotics photomineralization using CeO_2/ZnO composites are rare and limited to the degradation of carbamazepine [28], nizatidine [29], levofloxacin [27], acetaminophen [2] and ciprofloxacin. None of these studies has specified antibiotics mineralization mechanisms on CeO_2/ZnO heterostructures, and reactions have generally been limited by toxic by-products. In most studies performed on heterogeneous catalysis, no measurements have confirmed complete degradation of organic pollutants.

 doi:10.20944/preprints202306.1244.v1

Photodegradation of some toxic chemicals has been achieved under UV irradiation, but the few studies performed under visible light have shown poor photocatalytic efficiency. The limited mineralization activity of CeO_2/ZnO heterostructures has been linked to the nature of heterojunctions between the two oxides, and the number of radicals produced under UV light. Various techniques have been used for synthesizing ZnO/CeO_2 composites, such as hydrothermal/solvothermal and microwave synthesis, electrodeposition, precipitation, physical vapor deposition, chemical vapor deposition, micellar method, template-assisted synthesis etc.. For stabilizing Zn in CeO_2, and limiting its release, a $Ce_{1-x}Zn_xO_{2-x}$ solid solution has been prepared via a soft solution chemical route in the presence of citric acid as complexing agent for metal cations. This solid solution allows the construction of heterojunctions in $Ce_{1-x}Zn_xO_{2-x}$ oxygen vacancies for enhancing O_2 chemisorption and $Ce^{4+}\leftrightarrow Ce^{3+}$ electron conduction, further leading to easy photoexcited electron transfer [23]. Futhermore, existing abundant oxygen gaps can reduce electron-hole recombinations and enhance the photocatalytic mineralization of organic species. Moreover, photocatalytic reactions supported on ZnO, CeO_2 and their composite materials have been carried out only under ultraviolet light while there is the possibility of studying photo-excitation under visible light [23-27]. While most catalytic efficiencies obtained under UV are said to be good, the process is expensive, whereas the photo-excitation effect of visible/solar light is highly beneficial and can lead to significant degradation rates.

In the present work, several substitution rates of Ce^{4+} by Zn^{2+} in $Ce_{1-x}Zn_xO_{2-x}$ have been performed. The relationship between the photo-excitation mechanism, pollutant mineralization capacity and photocatalysts microstructure has been discussed. To the best of our knowledge, the photocatalytic behavior of either CeO_2/ZnO composites or a $Ce_{1-x}Zn_xO_{2-x}$ solid solution towards non-steroidal anti-inflammatory drugs in water, especially sodium diclofenac has never been described. Therefore, the present work is a pioneer work for Diclofenac photomineralization by $Ce_{1-x}Zn_xO_{2-x}$ solid solution catalysts under visible light.

2. Results and discussion

2.1. Structural Analysis

X-ray diffraction (XRD) analysis of the materials ZnO, CeO_2 and the solid solution $Ce_{1-x}Zn_xO_2$-x was performed to identify the corresponding crystal structures (Fig.2). The diffraction pattern of ZnO calcined at 700°C shows a zincite structure, while CeO_2 has a fluorine structure without any secondary phase in both cases. Combining these two oxides ZnO and CeO_2 produces the solid solution materials $Ce_{1-x}Zn_xO_{2-x}$ (x=0.1, 0.2, 0.3, 0.4) (Fig.2) with a crystalline structure typical of CeO_2. It should be noted that when the calcination temperature increases, the crystallinity improves with a slight shift of the XRD peaks towards the large angles, while preserving the fluorine structure. The quantity of CeO_2 being preponderant in the materials prepared, they retain the physical properties of cerium oxide. Indeed, the melting temperature of CeO_2 (2400°C) is higher than that of ZnO (1975°C) which suggests a good thermal resistance for CeO_2 due to higher crystallinity than ZnO. These explanations may favor the unique appearance of CeO_2 peaks on the diffractogram of $Ce_{1-x}ZnxO_{2-x}$ composite materials [23]. The variation of the intensity may be due to the difference in diffusion coefficients between the two cations Ce^{4+} and Zn^{2+} ($D_{Ce}>D_{Zn}$) in the final product structure.

Preprints (www.preprints.org) | NOT PEER-REVIEWED | Posted: 16 June 2023 doi:10.20944/preprints202306.1244.v1

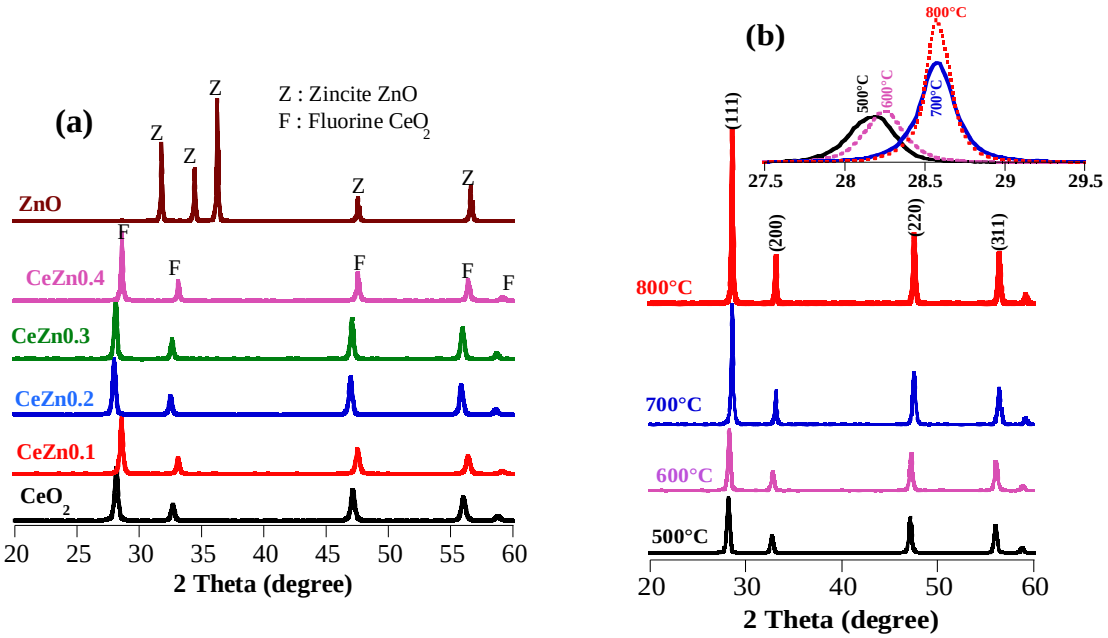

Figure 2. X–ray diffractogram of samples (a) CeZnx calcined at 700 °C and (b) CeZn0.1 calcined at different temperatures. "x" means the Zn content in the solid solution.

In order to further determine structural characteristics, the microstrain (δ) and dislocation density (ε) were calculated using equations 1 and 2 as follows:

$$\varepsilon = \frac{\beta}{4tan\theta} \quad \text{(Eq.1)}$$

$$\delta = \frac{1}{D^2} \quad \text{(Eq.2).}$$

The average crystallite size (D) was obtained by the Debye-Scherrer equation 3:

$$D = \frac{K\lambda}{\beta cos\theta} \quad \text{(Eq.3),}$$

where λ is the X-ray wavelength, q is a specific angle, β is the width at half maximum (FWHM) for the anatase peak (111), and k is the constant depending on the shape of the crystallites (k is 0.9 when the particles are spherical).

According to the results in **Figure 3**, the average crystallite size slightly increases with the calcination temperature and the inserted Zn content. This promotes the electronic and optical properties of the $Ce_{1-x}Zn_xO_{2-x}$ solid solution giving a periodic arrangement of Ce and Zn atoms in the fluorine crystal that not found in the CeO_2-ZnO composite reported elsewhere [27, 30, 31]. This arrangement of atoms affects microstrain (δ) and dislocation density (ε) (Table 1). Thus, a periodic heterojunction in the $Ce_{1-x}Zn_xO_{2-x}$ crystal lattice can be established.

Preprints (www.preprints.org) | NOT PEER-REVIEWED | Posted: 16 June 2023 doi:10.20944/preprints202306.1244.v1

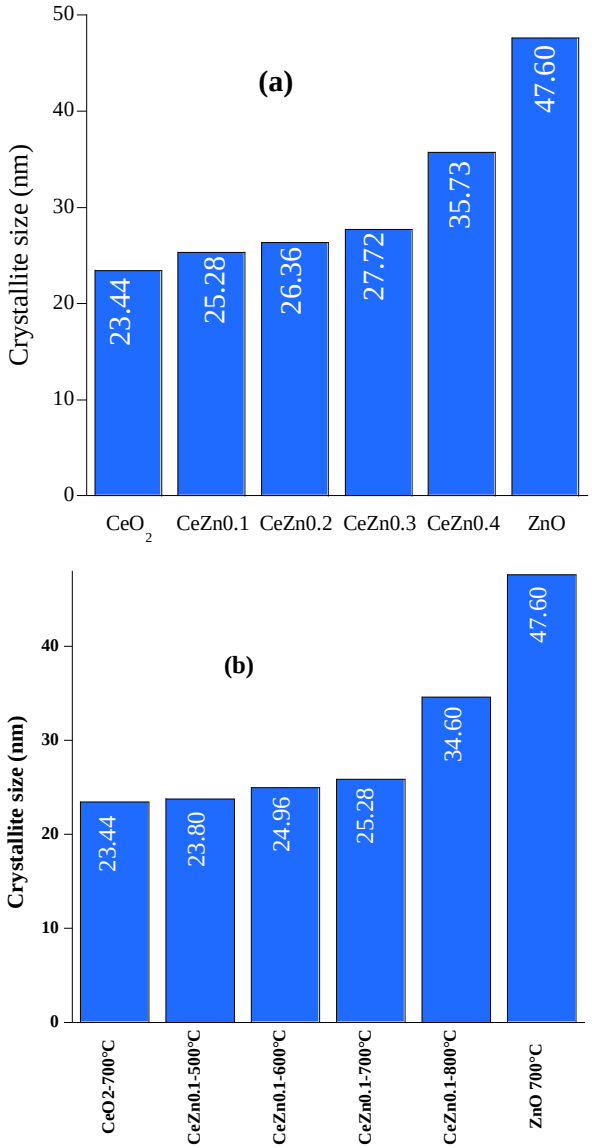

Figure 3. Crystallite sizes of samples **(a)** CeZnx calcined at 700°C; (b) CeZn0.1 calcined at different temperatures.

Table 1. Crystallographic parameters of synthesized materials.

		2θ (degree)	Microstrain (ε)	Dislocation density (δ)
CeO_2		28.16	0.617	1.820
$Ce_{1-x}Zn_xO_{2-x}$	0.1	28.58	0.589	1.505
	0.2	27.98	0.544	1.439
	0.3	28.10	0.518	1.301
	0.4	28.61	0.438	0.783
ZnO		36.17	0.236	0,441

Surface area and pore size are among the key indicators for good photocatalytic efficiency of materials. Thus, texture parameters of the different photocatalysts calcined at 700°C were determined using nitrogen (N_2) adsorption-desorption data at 77 k (Fig.4). The mesoporosity of the surface of the studied materials was confirmed by the presence of hysteresis. As shown in Table 2, the BET surface area of cerium oxide is 6.44 m^2g^{-1}, while the surface area of pure zinc oxide is 0.65 m^2g^{-1}. Interestingly, the surface area is higher for CeZn0.1 (S_{BET}= 8.05 m^2g^{-1}) than for ZnO and CeO_2. This increase could be due to a better dispersion and a decrease in the ZnO size inside the CeO_2 matrix which allows the extension of the network through hybrid bonds such as Zn-O-Ce. Pore size distribution shows

Preprints (www.preprints.org) | NOT PEER-REVIEWED | Posted: 16 June 2023 doi:10.20944/preprints202306.1244.v1

average pore diameters of 30, 70, and 41 nm for CeO_2, ZnO and CeZn0.1, respectively (Table 2).

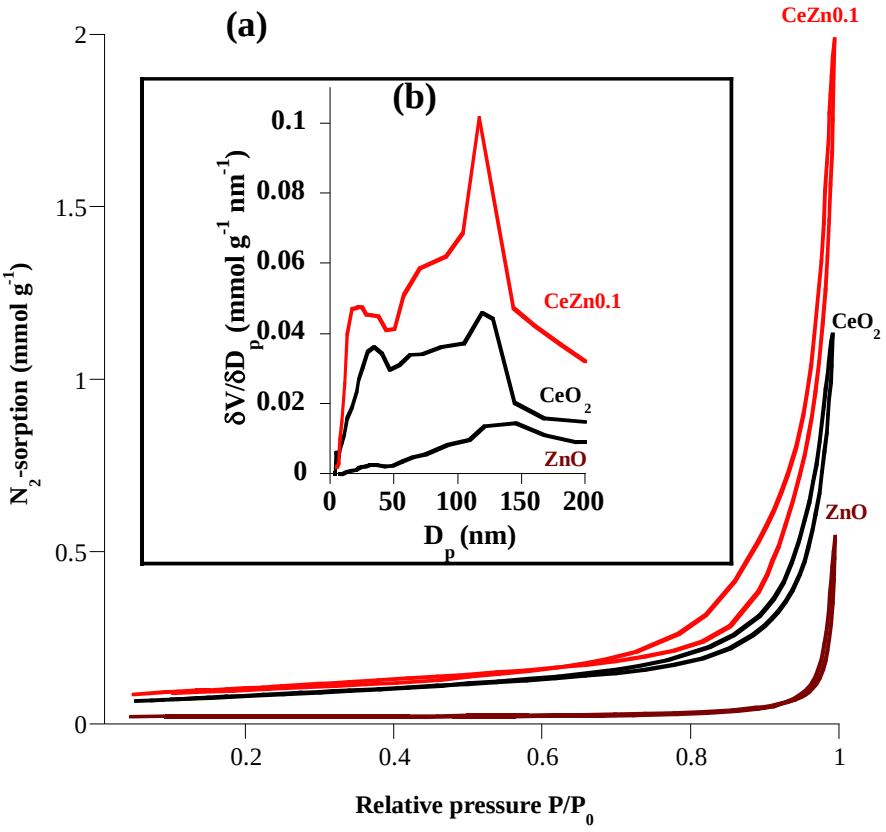

Figure 4. (a) N_2-adsortion/desorption curves and (b) pores size distribution of ZnO, CeO_2 and CeZn0.1 powders.

Table 2. Specific surface area (S_{BET}), pore volume (V_p) and average pore diameter (D_p) of the oxides ZnO, CeO_2 and CeZn0.1.

	ZnO	CeO_2	CeZn0.1
S_{BET} (m^2 g^{-1})	0.65	6.44	8.05
V_p (cm^3 g^{-1})	0.006	0.039	0.069
D_p (nm)	70.25	29.62	40.89

Surface morphologies of ZnO, CeO_2 and CeZnx oxides calcined at 700°C were studied by SEM (Fig. 5). ZnO particles are in the form of irregularly shaped elongated hexagons and quasi-spherical aggregated nanoparticles, while CeO_2 nanoparticles appear as amorphous agglomerates. However, the addition of ZnO to CeO_2 seems to affect the morphology and size of resulting nanocomposites. Fig. 5c and 5d clearly show a decrease in the size of CeZn0.1 elongated hexagons with a slight increase in the porosity.

Preprints (www.preprints.org) | NOT PEER-REVIEWED | Posted: 16 June 2023 doi:10.20944/preprints202306.1244.v1

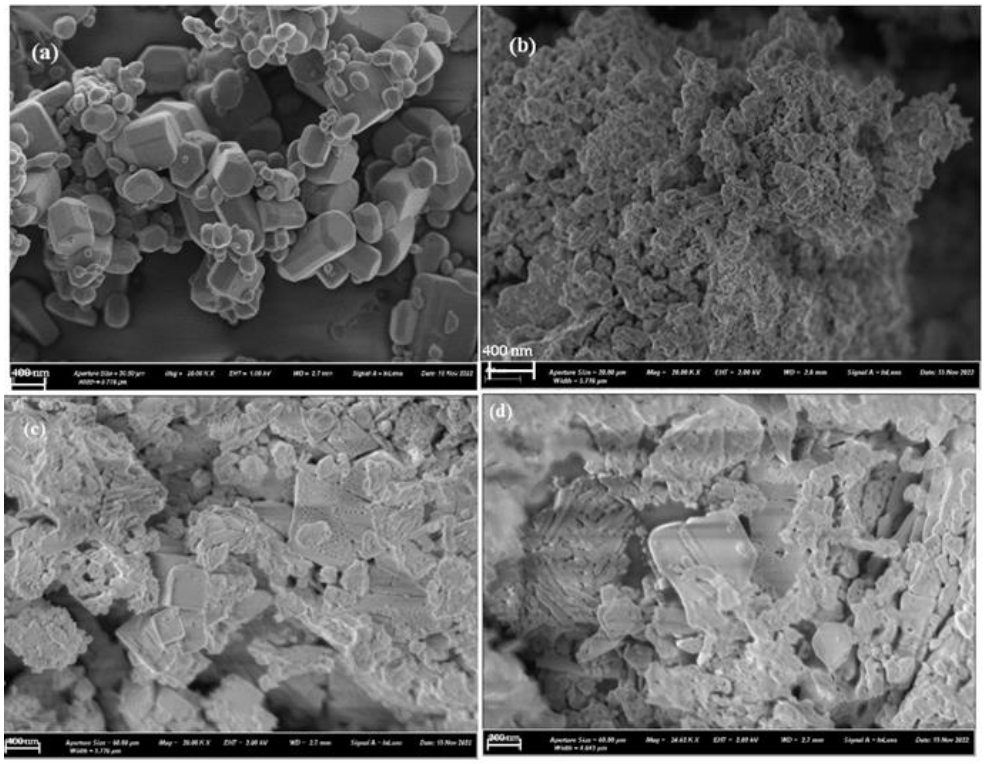

Figure 5. Scanning electron microscopy (SEM) of (a) ZnO, (b) CeO_2, (c) et (d) CeZn0.1.

XPS analysis was performed for determining the surface composition as well as the oxidation state of each material. This analysis shows the presence of O-Ce (Fig 6-d) and O-Zn bonds in CeO_2 modified by ZnO. CeZn0.1 calcined at 700°C (Fig 6a) shows the presence of three main peaks which are Zn_{2p} (1025.45 eV), O_{1s} (532.98 eV) and Ce_{3d} (886.47 eV) with a carbon standard peak C_{1S} (288.26 eV).

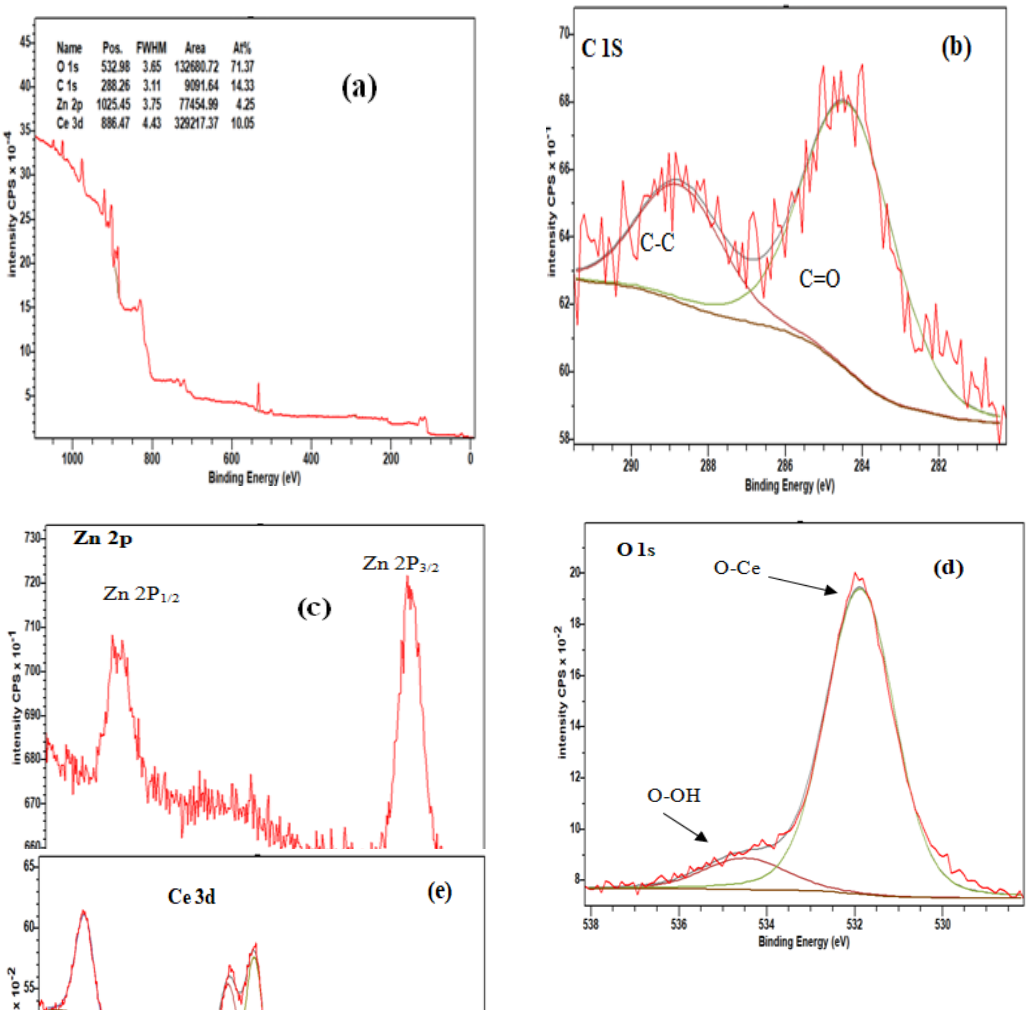

 doi:10.20944/preprints202306.1244.v1

Figure 6. XPS spectrum of typical CeZn0.1 powder calcined at 700°C.

Figure 6 also shows the deconvolution of the Zn_{2p} peak, which can be divided into two fitting peaks at about 1044.7 and 1020.6 eV attributed to $2p_{1/2}$ and $2p_{3/2}$ Zn orbitals, respectively, indicating that Zn valence is 2. The binding energy difference between the Zn-$2p_{1/2}$ and Zn-$2p_{3/2}$ orbitals is 23 eV, which confirms the presence of Zn^{2+} ions in the corresponding oxides. The deconvolution of the O_{1s} peak can be split into two peaks at 532.1 and 534.1 eV characteristic of the O-Ce and O-H bonds on the surface [31, 32]. Finally, the deconvolution of the Ce_{3d} peak shows six characteristic peaks for coherent bonds of Ce^{4+} ions. Due to structural and surface defects and a synergistic interaction between Zn-O and Ce-O, Therefore, XPS results confirmed the presence of Zn-O and Ce-O in CeZnx solid solution catalysts.

2.2. Optical properties

Optical properties of the prepared materials were determined by UV-vis diffuse reflectance spectroscopy (DRS) (Fig.7). Depending on the Zn content in the CeZnx solid solution, a distinct red shift of the UV-vis spectra was observed. The band gap energy (E_g) of synthesized photocatalysts was calculated using the following equation [31]:

$E_g = hc/\lambda_{max} = 1240/\lambda_{max}$, where h is Planck's constant, c is the speed of light and λ_{max} is the maximum wavelength.

Preprints (www.preprints.org) | NOT PEER-REVIEWED | Posted: 16 June 2023 doi:10.20944/preprints202306.1244.v1

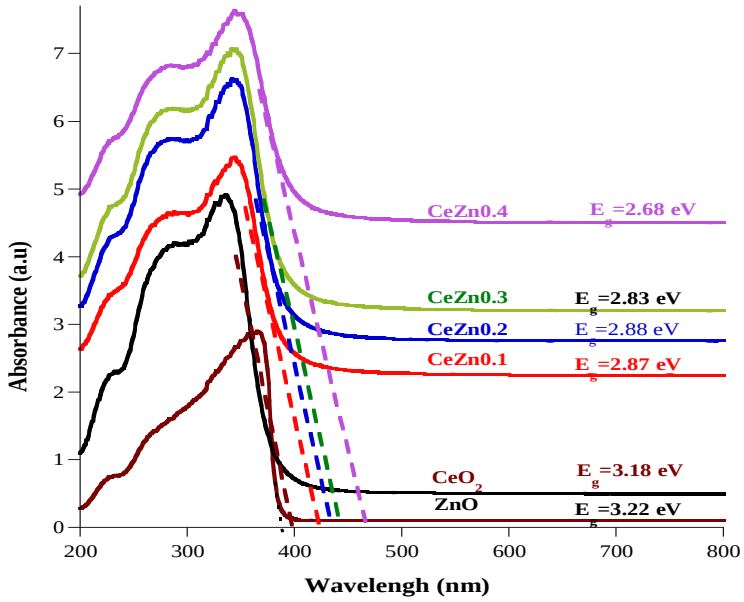

Figure 7. UV-vis absorption spectra of ZnO; CeO_2 and CeZn0.1.

Results indicate that gap energies of ZnO and CeO_2 are 3.22 eV and 3.18 eV, respectively, while the band gap of $CeZn_x$ materials is approximately 2.8 eV, excepted for CeZn40 which has a bandgap of 2.68 eV. The narrowing of the band gap is closely related to the concentration of oxygen vacancies when Zn is inserted into the $Ce_{1-x}Zn_xO_{2-x}$ solid solution [23]. These results also indicate that $CeZn_x$ catalysts can extend the absorption slope to larger wavelengths. That's why, these materials can be photoactivated under sunlight, which is very beneficial for improving photocatalytic mineralization properties.

2.3. Photocatalytic mineralization of diclofenac

The photocatalytic efficiency of solid solution materials $Ce_{1-x}Zn_xO_{2-x}$ (named $CeZn_x$) compared to CeO_2 and ZnO oxides was assessed for the degradation and mineralization of diclofenac in aqueous solution under UV-Visible irradiation (λ_{max}= 300-800 nm). In the absence of the catalyst, diclofenac was stable during sunlight irradiation and its photolysis was insignificant. It should be noticed that photocatalysis is coupled to the pollutant adsorption at the catalyst surface after diffuse migration close to this surface, and degradation rate is proportional to the recovery rate of active sites on the catalyst surface. Tests performed in the dark showed no significant reduction in the initial Diclofenac concentration. The decrease of Diclofenac concentration observed under sunlight showed the photocatalytic efficiency of the various produced photocatalysts. Lower photocatalytic activity was observed with solid solution materials $CeZn_x$, than with pure oxides (ZnO and CeO_2) (Fig.8a). In contrast, variations in total organic carbon showed a higher mineralization activity with $CeZn_x$ solid solution catalysts than with ZnO (no mineralisation) and CeO_2 (less than 20% mineralization after 2h irradiation) (Fig.8b). Optimal mineralization was observed with with $Ce_{0.9}Zn_{0.1}O_{1.9}$ catalyst, which showed about 65.50% Diclofenac mineralization and photodegradation only after 2 h irradiation.

This result strongly suggests that the small fraction of Zn in $Ce_{0.9}Zn_{0.1}O_{1.9}$ is offset by the presence of vacancies acting as determining factors in the essential step of drug mineralization. Indeed, while the insertion of Zn in the CeO_2 structure leads to structural defects, mineralization increases when the amount of inserted Zn decreases, and is optimal with CeZn0.1 catalyst.

Preprints (www.preprints.org) | NOT PEER-REVIEWED | Posted: 16 June 2023 doi:10.20944/preprints202306.1244.v1

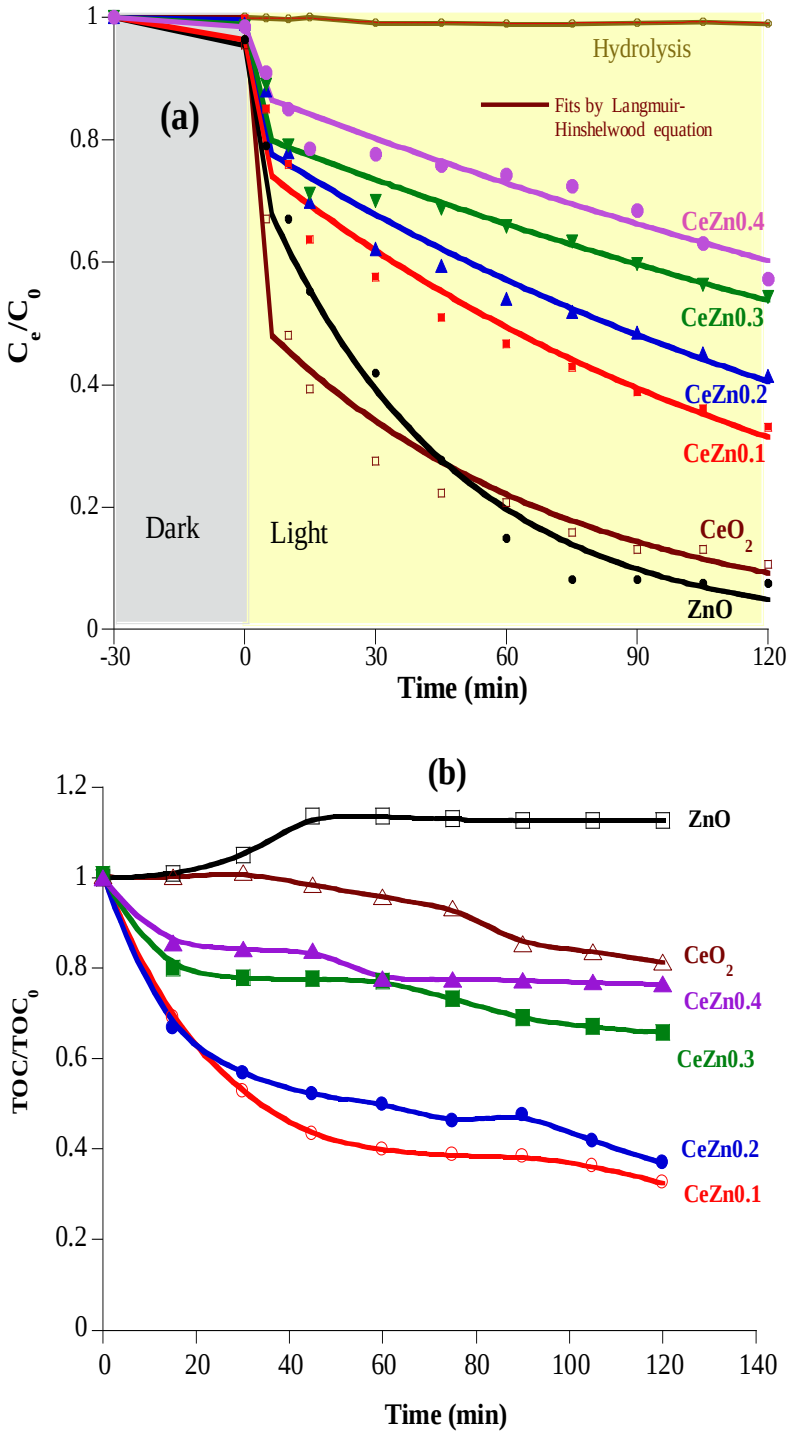

Figure 8. Effect of the Zn content of photocatalysts on the photocatalytic degradation (a) and mineralization (b) of Diclofenac. Controls: ZnO and CeO_2.

Heat treatment of $Ce_{0.9}Zn_{0.1}O_{0.9}$ has a significant effect on its photocatalytic activity (Fig 9). Catalyst calcined at 500 or 700°C show the highest photocatalytic activity (Fig 9a) and drug mineralization (Figure 9b). Consequently, the improved photocatalytic performance could be due to the heterojunction between the Ce-O and Zn-O bonds and the presence of oxygen vacancies that narrowed the band gap of the CeZnx solid solution materials.

Preprints (www.preprints.org) | NOT PEER-REVIEWED | Posted: 16 June 2023 doi:10.20944/preprints202306.1244.v1

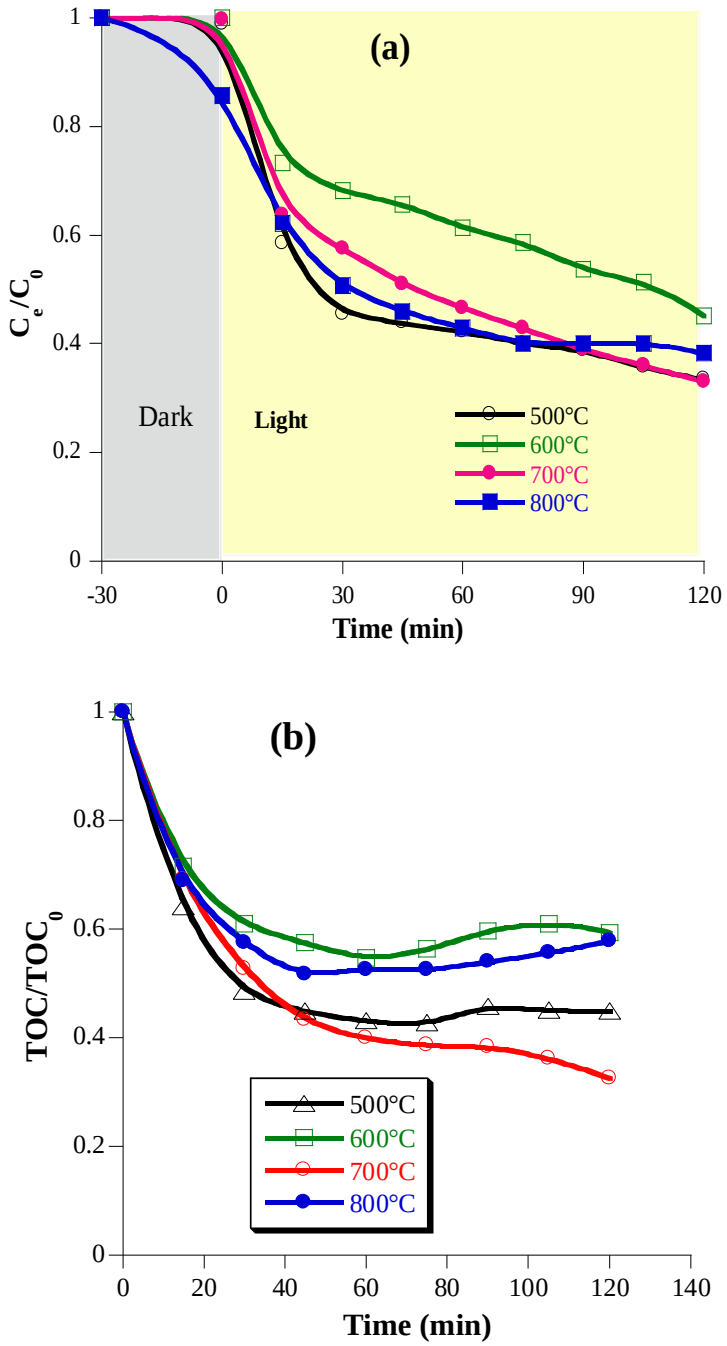

Figure 9. Effect of calcination temperature on (a) Photocatalytic degradation and (b) mineralization of sodium diclofenac in the presence of calcined CeZn0.1catalysts at different temperatures.

Due to the complexity of the photodegradation process, the mechanisms of action as well as the relative role of the different reactive species are not yet sufficiently elucidated. In the mechanism of photocatalysis, the oxidation of organic compounds can be carried out either by oxidizing radicals ($^{\bullet}OH$) produced by photoinduced positive charge carriers (h^+) or directly by the latter.

It is well known that -OH radicals are not only formed via holes in the valence band (VB), but also via electrons in the conduction band (CB). When oxygen O_2 is available and adsorbed on the surface of the catalyst, it can scavenge electrons from the BV to form superoxide radicals $O_2^{\bullet-}$. To clarify whether the degradation mechanism of diclofenac involves $^{\bullet}OH$, $^{\bullet}O_2^-$ radicals or holes, we performed scavenging experiments using specific

Preprints (www.preprints.org) | NOT PEER-REVIEWED | Posted: 16 June 2023 doi:10.20944/preprints202306.1244.v1

inhibitors for each of these active species. In this study, benzoquinone (BQ), ammonium oxalate (OA) and isopropanol (IPA) were added to the reaction solutions as scavengers for $O_2^{\bullet-}$radicals, h^+ holes, and $^{\bullet}OH$ radicals, respectively, at a concentration of 5 mmol/L before the catalyst addition. We used the same degradation process detailed earlier. After 2h irradiation, the concentration of Diclofenac decreased by 67, 54, 48 and 37 % without scavenger, with inhibition of $^{\bullet}OH$ radicals, h^+ holes and $O_2^{\bullet-}$radicals, respectively (**Figure 10)**. These results show that the relevance of active species in Diclofenac photocatalysis is as follows:

$O_2^{\bullet-}$radicals > h+ holes > $^{\bullet}OH$ radicals

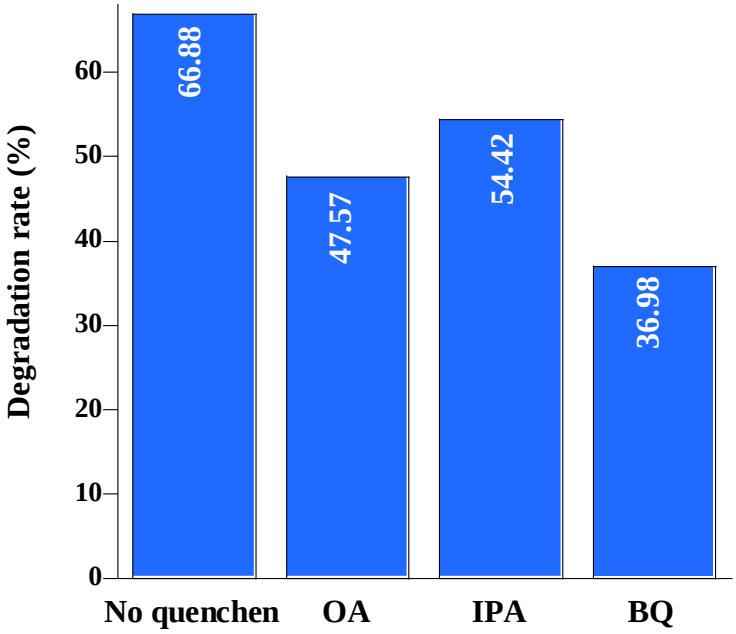

Figure 11. Effect of various active species scavengers on the photocatalytic degradation of Diclofenac by $Ce_{0.9}Zn_{0.1}O_{0.9}$ (C_0(DF) = 10 mg L^{-1}, catalyst dose = 2 g/L, C_P = 5 mmol/L, irradiation time = 2 h). Benzoquinone (BQ), ammonium oxalate (OA) and isopropanol (IPA) were added as scavengers for $O_2^{\bullet-}$radicals, h^+ holes, and $^{\bullet}OH$ radicals, respectively, at a concentration of 5 mmol/L before the catalyst addition.

In photocatalysis, the superoxide anion radical is formed by electrons and dissolved oxygen at the catalyst conduction band, while hydroxyl radical is generated from reactions between adsorbed water (or hydroxide ion) and holes at the valence band. Holes generated by the absorption of light at an appropriate wavelength can react directly with adsorbed diclofenac, but also water, leading to competition between these two reactions. Our results show that the indirect reduction of diclofenac via superoxide radical by electrons is the main photocatalytic mechnism. These results are in agreement with Liu *et al.* [33], which also concluded that $O_2^{\bullet-}$ was the main reactive species for the degradation of diclofenac.

3. Materials and Methods

3.1. Materials

All reagents used were of analytical grade and used without further purification. Zinc acetate dihydrate (≥99.0%), cerium (III) chloride heptahydrate (99.9%) citric acid (99%), sodium Diclofenac (Aldrich 98%) and ammonium hydroxide were supplied by Sigma aldrich.

3.2. Synthesis of ZnO, CeO_2 and $Ce_{1-x}Zn_xO_{2-x}$ solid solutions

Preprints (www.preprints.org) | NOT PEER-REVIEWED | Posted: 16 June 2023 doi:10.20944/preprints202306.1244.v1

Synthesis of ZnO nanoparticles was carried out by co-precipitation. Three grams of zinc acetate were dissolved in 20 ml of distilled water under magnetic stirring for 30 min. Then, 3.2 g of sodium carbonate was dissolved in 100 ml of water and added dropwise to the zinc acetate solution. The resulting mixture was stirred for 3 hours with pH control at pH 7. The white produced precipitate was filtered and dried in an oven at 105°C. The obtained powder was then calcined at 700°C in a muffle oven for 2 hours. It was ground with an agate mortar and stored in an airtight container at room temperature for further analysis.

Preparation of CeO_2 was carried out by dissolving 1.5 g of cerium chloride ($CeCl_3$) and 0.7698 g of citric acid in 20 ml of distilled water under magnetic stirring for 30 min. Then, ammonium hydroxide (NH_4OH) was dropwise added to the mixture at room temperature. The produced precipitate was left to ripen for 3 hours at room temperature, dried at 105°C in the oven for 24 hours without solid-liquid separation to preserve the metal ion contents introduced into the final product. Finally, the collected powder was ground and calcined for 2 hours, at temperatures between 500°C- 800°C.

The solution solid materials $Ce_{1-x}Zn_xO_{2-x}$ ((x=0, 0.1, 0.2, 0.3 and 0.4) were obtained by a similar procedure to that of pure CeO_2, except for adding a variable amounts of preformed ZnO powder to the solution containing Ce^{3+} ions. Finally, samples were calcined at 500°C, 60°C, 700°C and 800°C.

3.3. Methods of characterization

X-ray diffraction patterns were recorded with an X-ray a Ragaku Miniflex I diffractometer (CuKα cathode, λ= 0.154056 nm). Crystallite size was estimated by applying the Debye-Scherrer equation. SEM analyses were performed on an ion beam scanning electron microscope (JEOL 6700F equipped with a field emission gun with an extraction potential of 2.5 kV) associated with an EDX. The specific surface area (S_{BET}) was calculated from the Brunauer-Emmett-Teller (BET) equation from the physisorption of N_2 at 77 K. X-ray photoelectronic spectroscopy (XPS) measurements were performed on an Ultra Vacuum Spectrometer (UVH) equipped with a VSW class WA hemispheric electron analyzer. The X-ray source used was a double Al Kα (1486.6 eV) aluminum anode as incident radiation. The general high-resolution spectra were recorded in constant energy mode (100 and 20 eV, respectively). In order to correct for shift in binding energy due to electrostatic charge, the internal reference used was the C1s peak at 284.9 eV, characteristic of sp^2 hybridized C. The background was subtracted according to the Shirley method.

3.4. Evaluation of photocatalytic performance

An amount of 100 mg of the photocatalyst (0.5 g/L) was added to the sodium diclofenac solution (200 mL, 10 mg/L) in a 400 mL Pyrex beaker. The suspension was stirred in the dark for 30 minutes to reach the adsorption-desorption equilibrium. Then, the solution was irradiated with a SUNTEST CPS+ solar simulator with an air-cooled 1500 W xenon lamp (765 W/m^2, λ_{max}= 300-800 nm). The distance between the light source and the suspension was 20 cm. At regular irradiation intervals, samples were taken with a syringe followed by filtration with 0.22 µm millipore filters and then analyzed with a UV-vis spectrophotometer (ZUZI Spectrophometer model 4211/50) at 276 nm. The Total Organic Carbon (TOC) concentration was assessed with a Shimadzu model TOC-L. To demonstrate the efficiency of the catalyst, a direct photolysis of sodium diclofenac in water was performed by solar irradiation. It was carried out before any photocatalytic experiment to evaluate its contribution to the degradation of the chosen drug under the same operating conditions recommended for photocatalysis.

4. Conclusion

 doi:10.20944/preprints202306.1244.v1

In the present study, ZnO, CeO_2 and solid solution photocatalysts $Ce_{1-x}Zn_xO_{2-x}$ were synthesized and characterized. X-ray diffraction showed that CeO_2 and CeZnx (x=0.1, 0.2, 0.3, 0.4) display a fluorine structure, while ZnO has a zincite structure without any secondary phase. The fluorine structure of CeZn0.1 remained stable after calcination between 500 and 800°C, excepted for a slight shift of the lines towards large angles. Besides, XPS analysis showed several peaks attributable to the divalent character of Zn^{2+} and mainly to the quadrivalent character of Ce^{4+} , highlighting the Zn-O and Ce-O bonds. Lower gap energies of $CeZn_x$ solids than ZnO and CeO_2 are related to the presence of vacancies and electron transfer between cerium atoms. A synergy between the photodegradation and mineralization processes was carried out on Diclofenac under sunlight.

Author Contributions: Conceptualization, M.A. and D.R.; methodology, formal analysis, A.V.A., C.B.D.N.. and M.A..; investigation, M.A. and A.L.; writing—original draft preparation, M.A., D.R. and A.L.; writing—review and editing, M.A. and A.L..; visualization, A.V.A. and D.R.; supervision, D.R AND A.L..; project administration, D.R.; funding acquisition, A.L. and D.R. All authors have read and agreed to the published version of the manuscript.

Funding: This research was funded by Campusfrance Toubkal grant no. 21/128: 45776SK.

Data Availability Statement: Not applicable.

Conflicts of Interest: The authors declare no conflict of interest.

References

[1] E.N. Evgenidou, I.K. Konstantinou, D.A. Lambropoulou, Occurrence and removal of transformation products of PPCPs and illicit drugs in wastewaters: a review, Science of the Total Environment. 505 (2015) 905–926.

[2] N. Nakada, H. Shinohara, A. Murata, K. Kiri, S. Managaki, N. Sato, H. Takada, Removal of selected pharmaceuticals and personal care products (PPCPs) and endocrine-disrupting chemicals (EDCs) during sand filtration and ozonation at a municipal sewage treatment plant, Water Research. 41 (2007) 4373–4382.

[3] C.B. Dantio Nguela, N.H. Manga, C. Marchal, A.V. Abega, N.J. Nsami, D. Robert, Effect of Biogenic Silica Behavior in the Incorporation of Mesoporous Anatase TiO_2 for Excellent Photocatalytic Mineralization of Sodium Diclofenac, Catalysts. 12 (2022) 1001

[4] J. Hofmann, U. Freier, M. Wecks, S. Hohmann, Degradation of diclofenac in water by heterogeneous catalytic oxidation with H_2O_2, Applied Catalysis B: Environmental 70 (2007) 447–451.

[5] E. Rosales, S. Diaz, M. Pazos, M.A. Sanromán, Comprehensive strategy for the degradation of anti-inflammatory drug diclofenac by different advanced oxidation processes, Separation and Purification Technology 208 (2019) 130–141.

[6] J. An, Q. Zhou, Degradation of some typical pharmaceuticals and personal care products with copper-plating iron doped Cu_2O under visible light irradiation, Journal of Environmental Sciences. 24 (2012) 827–833.

[7] R. Daghrir, P. Drogui, D. Robert, Modified TiO_2 for environmental photocatalytic applications: a review, Industrial & Engineering Chemistry Research. 52 (2013) 3581–3599.

[8] A. Pruna, Z. Wu, J. Zapien, Y. Li, A. Ruotolo, Enhanced photocatalytic performance of ZnO nanostructures by electrochemical hybridization with graphene oxide, Applied Surface Science. 441 (2018) 936–944.

[9] A. Rahman, A. Jalil, S. Triwahyono, A. Ripin, F. Aziz, N. Fatah, N. Jaafar, C. Hitam, N. Salleh, N. Hassan, Strategies for introducing titania onto mesostructured silica nanoparticles targeting enhanced photocatalytic activity of visible-light-responsive Ti-MSN catalysts, Journal of Cleaner Production. 143 (2017) 948–959.

[10] J. Liu, B. Wang, Z. Li, Z. Wu, K. Zhu, J. Zhuang, Q. Xi, Y. Hou, J. Chen, M. Cong, Photo-Fenton reaction and H_2O_2 enhanced photocatalytic activity of α-Fe_2O_3 nanoparticles obtained by a simple decomposition route, Journal of Alloys and Compounds. 771 (2019) 398–405.

[11] A. Meng, B. Zhu, B. Zhong, L. Zhang, B. Cheng, Direct Z-scheme TiO_2/CdS hierarchical photocatalyst for enhanced photocatalytic H_2-production activity, Applied Surface Science. 422 (2017) 518–527.

[12] J.B. Baxter, C.A. Schmuttenmaer, Conductivity of ZnO nanowires, nanoparticles, and thin films using time-resolved terahertz spectroscopy, The Journal of Physical Chemistry B. 110 (2006) 25229–25239.

[13] E.A. Meulenkamp, Electron transport in nanoparticulate ZnO films, The Journal of Physical Chemistry B. 103 (1999) 7831–7838.

[14] K.M. Lee, C.W. Lai, K.S. Ngai, J.C. Juan, Recent developments of zinc oxide based photocatalyst in water treatment technology: a review, Water Research. 88 (2016) 428–448.

[15] N. Yusoff, L.-N. Ho, S.-A. Ong, Y.-S. Wong, W. Khalik, Photocatalytic activity of zinc oxide (ZnO) synthesized through different methods, Desalination and Water Treatment. 57 (2016) 12496–12507.

[16] M. Kositzi, I. Poulios, K. Samara, E. Tsatsaroni, E. Darakas, Photocatalytic oxidation of cibacron yellow LS-R, Journal of Hazardous Materials. 146 (2007) 680–685.

 doi:10.20944/preprints202306.1244.v1

[17] Y. Wang, H.-B. Fang, Y.-Z. Zheng, R. Ye, X. Tao, J.-F. Chen, Controllable assembly of well-defined monodisperse Au nanoparticles on hierarchical ZnO microspheres for enhanced visible-light-driven photocatalytic and antibacterial activity, Nanoscale. 7 (2015) 19118–19128.

[18] W. Yu, D. Xu, T. Peng, Enhanced photocatalytic activity of gC 3 N 4 for selective CO2 reduction to CH 3 OH via facile coupling of ZnO: a direct Z-scheme mechanism, Journal of Materials Chemistry A. 3 (2015) 19936–19947.

[19] R. Zha, R. Nadimicherla, X. Guo, Ultraviolet photocatalytic degradation of methyl orange by nanostructured TiO_2/ZnO heterojunctions, Journal of Materials Chemistry A. 3 (2015) 6565–6574.

[20] M. Ebrahimi, M. Samadi, S. Yousefzadeh, M. Soltani, A. Rahimi, T. Chou, L.-C. Chen, K.-H. Chen, A.Z. Moshfegh, Improved solar-driven photocatalytic activity of hybrid graphene quantum dots/ZnO nanowires: a direct Z-scheme mechanism, ACS Sustainable Chemistry & Engineering. 5 (2017) 367–375.

[21] Y. Ma, Y. Bian, Y. Liu, A. Zhu, H. Wu, H. Cui, D. Chu, J. Pan, Construction of Z-scheme system for enhanced photocatalytic H2 evolution based on CdS quantum dots/CeO_2 nanorods heterojunction, ACS Sustainable Chemistry & Engineering. 6 (2018) 2552–2562.

[22] M. Haneda, T. Kaneko, N. Kamiuchi, M. Ozawa, Improved three-way catalytic activity of bimetallic Ir–Rh catalysts supported on CeO_2/ZrO_2, Catalysis Science & Technology. 5 (2015) 1792–1800.

[23] R. Li, S. Yabe, M. Yamashita, S. Momose, S. Yoshida, S. Yin, T. Sato, UV-shielding properties of zinc oxide-doped ceria fine powders derived via soft solution chemical routes, Materials Chemistry and Physics 75 (2002) 39-44.

[24] Z. Xiong, Z. Lei, Z. Xu, X. Chen, B. Gong, Y. Zhao, H. Zhao, J. Zhang, C. Zheng, Flame spray pyrolysis synthesized ZnO/CeO_2 nanocomposites for enhanced CO2 photocatalytic reduction under UV–Vis light irradiation, Journal of CO_2 Utilization 18 (2017) 53-61.

[25] L. Zhu, H. Li, P. Xia, Z. Liu, D. Xiong, Hierarchical ZnO Decorated with CeO_2 Nanoparticles as the Direct Z-Scheme Heterojunction for Enhanced Photocatalytic Activity, ACS Appl. Mater. Interfaces. 10 (2018) 39679–39687.

[26] I.-Tsan Liu, Min-Hsiung Hon, L. G. Teoh, The preparation, characterization and photocatalyticactivity of radical-shaped CeO_2/ZnO microstructures Ceramics International 40 (2014) 4019-4024.

[27] E. Cerrato, N. P. Ferreira- Gonçalves, P. Calza, M. C. Paganini, Comparison of the photocatalytic activity of ZnO/CeO_2 and ZnO/Yb_2O_3 mixed systems in the phenol removal from water: A mechanicistic approach, *Catalysts 10* (2020) 1222; https://doi.org/10.3390/catal10101222.

[28] P. Caregnato, K.R. Espinosa Jimenez, P.I. Villabrille, Ce-doped ZnO as photocatalyst for carbamazepine degradation, Catal. Today. (2020), https://doi. org/10.1016/j.cattod.2020.07.031 article in press

[29] R. Al Abri, F. Al Marzouqi, A.T. Kuvarega, M.A. Meetani, S.M.Z. Al Kindy, S. Karthikeyan, Y. Kim, R. Selvaraj, Nanostructured cerium-doped ZnO for photocatalytic degradation of pharmaceuticals in aqueous solution, J. Photochem. Photobiol. A Chem. 384 (2019), 112065.

[30] L. Wolski, K. Grzelak, M. Muńko, M. Frankowski, T. Grzyb, G. Nowaczyk, Insight into photocatalytic degradation of ciprofloxacin over CeO_2/ZnO nanocomposites: Unravelling the synergy between the metal oxides and analysis of reaction pathways, Applied Surface Science 563 (2021) 150338.

[31] Q. Zhang, X. Zhao, L. Duan, H. Shen, R. Liu, Controlling oxygen vacancies and enhanced visible light photocatalysis of CeO_2/ZnO nanocomposites, Journal of Photochemistry and Photobiology A: Chemistry 392 (2020) 112156.

[32] Z. Wang, P.Zhao, Y.Cheng, L. Liao, S. Li, Y.Luo , Z. Peng , P.Lin, D. He, Cerium oxide immobilized reduced graphene oxide hybrids with excellent microwave absorbing performance, Phys. Chem. Chem. Phys. 20 (2018) 14155-14165.

[33] X. Liu, F. Li, Y. Liu, P. Li, L. Chen, B. Li, T. Qian, W. Liu, Degradation of diclofenac in a photosensitization-like photocatalysis process using palladium quantum dots deposited graphite carbon nitride under solar light, J. of Env. Chem. Eng.10 (2022) 107545-107458